J. Fluid Mech. (1980), *vol.* 99, *part* 3, *pp.* 597–618
Printed in Great Britain

The formation of ripples and dunes on an erodible bed

By KELVIN J. RICHARDS

Department of Applied Mathematics and Theoretical Physics,
University of Cambridge, Silver Street, Cambridge CB3 9EW

(Received 28 August 1979)

A two-dimensional stability analysis is presented of flow of low Froude number over an erodible bed. Particular regard is given to the modelling of the turbulent flow close to the bed. In contrast to previous theories that use a constant eddy-viscosity approach the present theory predicts the occurrence of two separate modes of instability, with wavelengths related to the roughness of the bed and the depth of the flow. It is postulated that these two modes correspond to the formation of ripples and dunes respectively. The results are strongly dependent on the two parameters z_0, the roughness length of the bed, and β, the effect of the local bed slope on the bed-load transport. Using physically plausible estimates for these parameters the results of the analysis are in good agreement with observations for both ripples and dunes.

1. Introduction

A striking feature of transverse bed forms on an erodible bed, particularly for low-Froude-number flows, is the occurrence of two separate modes of growth of a bed wave. There is a distinct difference in the dimensions of the two forms (see, for example, Allen 1970). As a definition we shall classify those bed forms whose dimensions are dependent on the flow depth as dunes and those dependent solely on the local bed properties as ripples. In the sea and in some deeper rivers a further transverse bed form frequently occurs, commonly named mega-ripples. These features are similar in shape to the small-scale ripples but have larger dimensions, typically of wavelength 1–10 m.

Theories for the formation of the two types of bed form have often been treated separately. For a comprehensive review the reader is referred to the recent paper by Reynolds (1976). Kennedy (1963) treats the problem of the formation of dunes as a two-dimensional stability analysis. Using the potential flow solution for the flow over the perturbed bed, he relates the sediment transport to the local fluid velocity. To produce unstable waves he introduces a quantity, δ, which he defines as the distance by which the local sediment transport lags behind the local velocity at the bed. Exner (1925) had shown earlier, using a hydraulic model, that with the inclusion of friction there is a phase lag between the bed form and the fluid velocity, and thus sediment transport. By including friction in the flow and using specific representations for the bed load and suspended load, Engelund (1970) was able to predict the lag distance and obtain lower and upper bed-form regimes. Smith (1970) used the same approach but restricted the flow to a low Froude number. Fredsøe (1974) extended the work of Engelund by introducing the effect of the local bed slope on the bed-load rate. At low

0022–1120/80/4502-1630 $02.00

Froude numbers this was found to restrict the unstable waves to low wavenumbers and Fredsøe obtained good agreement between his theory and experimental results.

The formation of ripples is not so well understood and there is no general consensus of opinion. The various theories can be broadly divided into stability theories and theories involving the propagation of ripples downstream from an initial disturbance. Bagnold (1956) considers the stability of the bed. He defines a critical value of the Shields number above which all the surface grains are in a saltating motion. At slightly lower values of the Shields number he argues that the plane bed is unable to resist the applied shear stress. Primary ripples are then formed to create form drag and thus reduce the skin friction. For increasing flow conditions these primary ripples become unstable and form secondary ripples with a larger form drag. Liu (1957) proposes that the sediment bed acts as a viscous fluid and that ripples are a form of a Kelvin–Helmholtz type instability of two sheared fluids of different density. In contrast Raudkivi (1966) attributes ripples to a propagation downstream of an initial chance piling up of the sediment. Williams & Kemp (1971) purpose that these small deformations are caused by the random action of high turbulent velocities, or 'bursts', close to the bed. The deformation then causes the flow to separate with subsequent building up of the disturbance into a ripple. Ripple propagation proceeds by an erosion and deposition process downstream of the initial ripple.

The present paper presents a single linear stability theory of a plane erodible bed to account for the occurrence of both ripples and dunes. Only the bed-load transport of sediment is considered, restricting the analysis to flows with low shear rates. The theory is an extension of that of Engelund (1970) to include a more realistic description of the turbulent flow close to the bed. In particular the turbulent length scale of the flow is here assumed to increase linearly with height above the bed. The result is that two separate instability modes are found, one dependent on the local roughness of the bed and the other dependent on the depth of flow. The theory can also account for the formation of the large mega-ripples.

In §2 the linearized equations for a turbulent open channel flow over a small-amplitude bed wave are formulated. By relating the bed-load transport of sediment to the surface shear stress predicted by the model, the stability of the bed wave is examined in §3. The results of the analysis are presented in §4. These are compared with observations in §5 and a discussion of the results is presented in §6.

2. Open channel flow over a small-amplitude bed wave

To determine the stability of an erodible bed we require the flow over a small perturbation to the bed and to relate this to the transport of sediment, and thus the evolution of the perturbed bed. The bed displacement is given by

$$h = h_0 \exp i(kx - \sigma t) \tag{2.1}$$

where k is the wavenumber of the bed and σ its growth rate. We assume that the flow responds relatively rapidly to the slow development of the bottom wave, and therefore that the time dependence of the flow can be neglected. The validity of this assumption is tested in §6. The only interaction between the flow and the moving sediment will be through the possible modification of the roughness of the bed (see §5). In the tidal situation we shall assume that the flow can be assumed steady and the total effect of

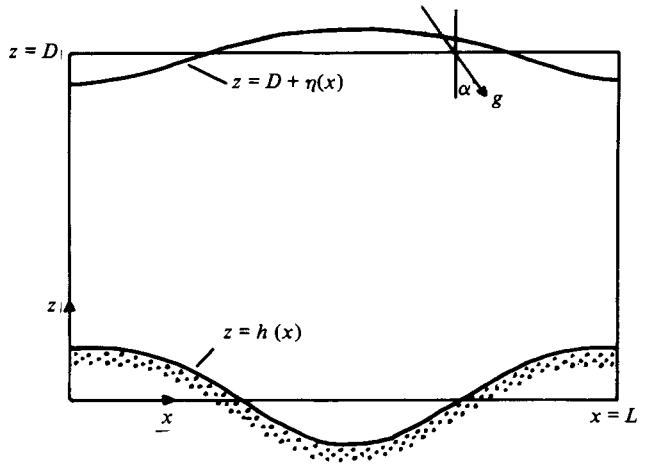

FIGURE 1. Definition sketch of flow region.

the tide found by integrating over the tidal cycle. This assumes that the development time of the flow is short compared with the tidal period, but it should also be noted that the majority of the sediment transported will take place when the stress is greatest, i.e. when the tidal flow is fully developed.

We consider a steady flow of depth D over a small periodic two-dimensional perturbation to the bed $h = h_0 \exp(ikx)$ driven either by an externally applied horizontal pressure gradient or by tilting the region through a small angle α (figure 1). The x and z co-ordinates are taken along and normal to the mean bed level respectively. The equations of motion for the mean velocity are then

$$\left.\begin{aligned} U\frac{\partial U}{\partial x} + W\frac{\partial U}{\partial z} &= -\frac{\partial p}{\partial x} + \frac{\partial}{\partial x}\tau_{xx} + \frac{\partial}{\partial z}\tau_{xz} + g\sin\alpha, \\ U\frac{\partial W}{\partial x} + W\frac{\partial W}{\partial z} &= -\frac{\partial p}{\partial z} + \frac{\partial}{\partial x}\tau_{xz} + \frac{\partial}{\partial z}\tau_{zz}, \end{aligned}\right\} \tag{2.2}$$

and the continuity equation

$$\frac{\partial U}{\partial x} + \frac{\partial W}{\partial z} = 0. \tag{2.3}$$

Here U, W are the components of the mean velocity in the x, z directions respectively, p is pressure, τ_{xz}, etc. are the Reynolds stresses and g the acceleration due to gravity.

We shall linearize the equations with respect to the wave slope $h_0 k$. Taylor, Richards & Nunes (1978) compare the results of the present linear theory with those of a numerical model which retains the nonlinear inertial terms and use the same turbulence closure. As an estimate of the effects of the linearization of the equations they find that the predictions of the two models of the perturbed surface shear stress and pressure differ by approximately 10 % for $h_0 k = 0{\cdot}05$ with the linear model overestimating the flow perturbations due to the wave at this amplitude.

In linearizing the problem a difficulty arises at the bottom boundary because of the logarithmic nature of the velocity profile of a turbulent flow near the bed. Engelund (1970) by introducing a slip velocity is able to use a Taylor expansion around $z = 0$

to obtain a boundary condition at $z = 0$. This is invalid in our case, however, because of the singularity of the velocity profile $U \sim \ln z$ at $z = 0$. This difficulty was noted by Miles (1957) and Benjamin (1959). Townsend (1972) assumes a logarithmic velocity profile near the surface and applies the bottom boundary condition above the wave. However, as noted by Taylor *et al.* (1978) his expansion of $\ln[(z-h)/z]$ requires $z \gg h_0$, restricting the results to very small values of the wave slope, $h_0 k \ll 0{\cdot}01$.

To overcome these difficulties we shall use a transformation of the co-ordinate system from (x, z) to (x^*, z^*) similar to that used by Taylor (1977).

The new co-ordinate system is defined by

$$x^* = x, \quad z^* = z - h_0 \exp(ikx) F(z^*). \tag{2.4}$$

We choose F so that the lines $z^* =$ constant are approximately streamlines and for the lines $z^* = 0$ and $z^* = D$ to correspond to the lower and unperturbed upper boundaries. The potential flow solution suggests the use of

$$F(z^*) = \frac{\sinh k(D-z^*)}{\sinh kD}. \tag{2.5}$$

Note that, on $z^* = 0$, $F = 1$ so that $z = h_0 \exp ikx$ and, on $z^* = D$, $z = D$.

In the non-orthogonal (x^*, z^*) co-ordinate system, retaining U and W as the downstream and normal Cartesian velocity components, equations (2.2) and (2.3) become

$$U\frac{\partial U}{\partial x^*} + \left(U\frac{\partial z^*}{\partial x} + W\frac{\partial z^*}{\partial z}\right)\frac{\partial U}{\partial z^*} = -\left(\frac{\partial}{\partial x^*} + \frac{\partial z^*}{\partial x}\frac{\partial}{\partial z^*}\right)p + \left(\frac{\partial}{\partial x^*} + \frac{\partial z^*}{\partial x}\frac{\partial}{\partial z^*}\right)\tau_{xx} + \frac{\partial z^*}{\partial z}\frac{\partial}{\partial z^*}\tau_{xz} + g\sin\alpha, \tag{2.6}$$

$$U\frac{\partial W}{\partial x^*} + \left(U\frac{\partial z^*}{\partial x} + W\frac{\partial z^*}{\partial z}\right)\frac{\partial W}{\partial z^*} = -\frac{\partial z^*}{\partial z}\frac{\partial p}{\partial z^*} + \left(\frac{\partial}{\partial x^*} + \frac{\partial z^*}{\partial x}\frac{\partial}{\partial z^*}\right)\tau_{xz} + \frac{\partial z^*}{\partial z}\frac{\partial}{\partial z^*}\tau_{zz} \tag{2.7}$$

and

$$\left(\frac{\partial}{\partial x^*} + \frac{\partial z^*}{\partial z}\frac{\partial}{\partial z^*}\right)U + \frac{\partial z^*}{\partial z}\frac{\partial W}{\partial z^*} = 0, \tag{2.8}$$

where to first order in wave slope

$$\frac{\partial z^*}{\partial z} = 1 - h_0 F' e^{ikx^*},$$

$$\frac{\partial z^*}{\partial x} = -ikh_0 F e^{ikx^*}$$

and the prime denotes differentiation with respect to z^*.

To close the above system of equations we need to express the Reynolds stresses in terms of mean-flow quantities. We shall use an eddy-viscosity approach based on an additional equation for the turbulent kinetic energy (see Rodi 1978). For a small perturbation to the bed the exact specification of the turbulent stresses should be unimportant provided the flow close to the bed is correctly modelled. We have chosen the present closure scheme in preference to a mixing-length hypothesis, to avoid the difficulties of the free surface where the stress is zero, and to that of Bradshaw,

Ferris & Atwell (1967) because of the need to specify zero turbulent energy at the free surface. However, similar results to those presented are expected with either of these alternative schemes. The fundamental difference between this and previous bed-stability theories (e.g. Fredsøe 1974; Smith 1970) is that the turbulence length scale of the flow close to the bed is assumed to increase linearly with height.

Following Taylor (1977) we assume that

$$\tau_{xz} = K\left(\frac{\partial U}{\partial z}+\frac{\partial W}{\partial x}\right),$$

$$\tfrac{2}{3}E+\tau_{xx} = K\left(\frac{\partial U}{\partial x}-\frac{\partial W}{\partial z}\right),$$

$$\tfrac{2}{3}E+\tau_{zz} = K\left(\frac{\partial W}{\partial z}-\frac{\partial U}{\partial x}\right)$$

and

$$\tfrac{2}{3}E+\tau_{yy} = 0,$$

where K is an eddy viscosity and $E = \frac{1}{2}(\overline{u'^2}+\overline{v'^2}+\overline{w'^2})$ the turbulent kinetic energy with $\overline{u'^2} = -\tau_{xx}$, etc. the components of the turbulence intensity.

The eddy viscosity is expressed as

$$K = l(\lambda E)^{\frac{1}{2}},$$

where l is a mixing length which is taken as a prescribed function of position and λ is a constant equal to the equilibrium value of $-\overline{u'w'}/E$ in the constant stress layer and given the value 0·25.

The turbulent energy, E, is determined by the transport equation (in x^*, z^* co-ordinates)

$$U\left(\frac{\partial}{\partial x^*}+\frac{\partial z^*}{\partial x}\frac{\partial}{\partial z^*}\right)E+W\frac{\partial z^*}{\partial z}\frac{\partial E}{\partial z^*}$$

$$= -\left(\frac{\partial}{\partial x^*}+\frac{\partial z^*}{\partial x}\frac{\partial}{\partial z^*}\right)[-\overline{u'p'}-\overline{u'E'}]+\frac{\partial z^*}{\partial z}\frac{\partial}{\partial z^*}[-\overline{w'p'}-\overline{w'E'}]-\overline{u'^2}\left(\frac{\partial}{\partial x^*}+\frac{\partial z^*}{\partial x}\frac{\partial}{\partial z^*}\right)U$$

$$-\overline{u'w'}\left(\frac{\partial z^*}{\partial z}\frac{\partial U}{\partial z^*}+\left(\frac{\partial}{\partial x^*}+\frac{\partial z^*}{\partial x}\frac{\partial}{\partial z^*}\right)W\right)-\overline{w'^2}\frac{\partial z^*}{\partial z}\frac{\partial W}{\partial z^*}-\epsilon. \quad (2.9)$$

The additional closure assumptions we shall make are

$$\overline{u'p'}+\overline{u'E'} = -K_E\frac{\partial E}{\partial x}$$

and

$$\overline{w'p'}+\overline{w'E'} = -K_E\frac{\partial E}{\partial z},$$

where K_E is assumed equal to K.

The dissipation of turbulent kinetic energy, ϵ, is represented by

$$\epsilon = (\lambda E)^{\frac{3}{2}}/l_D,$$

where the dissipation length scale l_D is taken to equal l.

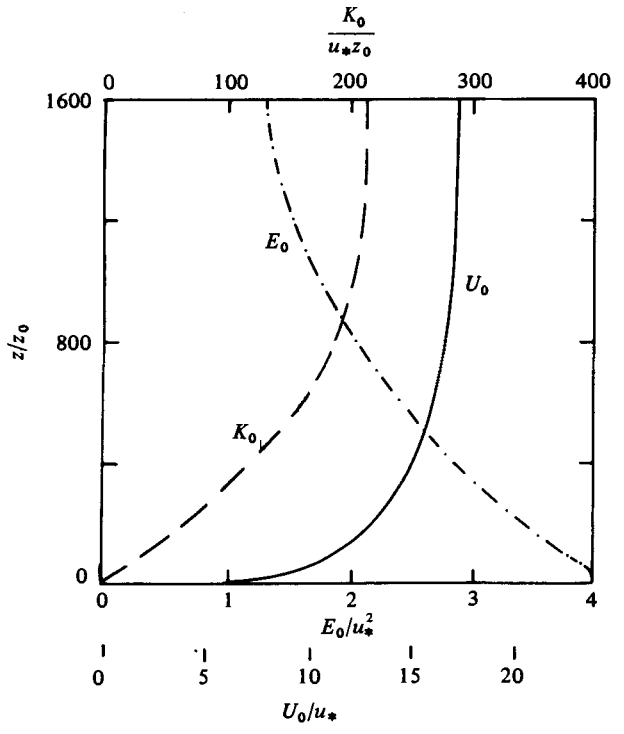

FIGURE 2. Unperturbed profiles of mean velocity, U_0, turbulent energy E_0 and eddy viscosity K_0; $D/z_0 = 1600$.

The mixing length l is taken as

$$l = l_0(z^*) + G(z^*) h_0 e^{ikx^*},$$

where

$$l_0(z^*) = \kappa(z^* + z_0)\left(1 - \frac{2}{3}\frac{z^*}{D}\right)^{\frac{1}{2}};$$

z_0 the roughness length of the bed and κ is von Kármán's constant, taken to be 0·4. The term

$$G(z^*) = (F - 1)\, l_0'(z^*)$$

is included so that, to first order in $h_0 k$, the mixing length is dependent on the normal distance from the bed near the lower boundary and dependent on z^* well away from the lower boundary. This form of mixing length gives $l_0 \sim \kappa(z^* + z_0)$ close to the surface and $l_0' = 0$ at $z^* = D$ with the eddy viscosity approximately constant in the upper half of the flow. Alternative forms of the mixing length have been tried (see Richards 1978), producing little change in the predicted surface shear stress and giving similar results for the stability analysis.

The undisturbed profiles of velocity $U_0(z)$ and turbulent energy $E_0(z)$ can be obtained from the reduction of the equations for flow over a plane bed, i.e.

$$\frac{\tau_0^2}{K} + \frac{d}{dz}\left(K \frac{d}{dz} E_0\right) - \frac{(\lambda E_0)^{\frac{3}{2}}}{l} = 0$$

and

$$\frac{dU}{dz} = \frac{\tau_0}{K},$$

where τ_0 is the unperturbed horizontal shear stress given by

$$\tau_0(z) = u_*^2(1-z/D)$$

and $u_*^2 = gD\sin\alpha$, the friction velocity. The boundary conditions taken are $U_0 = 0$ on $z = 0$ and $dE_0/dz = 0$ on $z = 0$ and $z = D$ to allow no diffusion of turbulent energy through the boundaries. Profiles of $U_0(z)$, $E_0(z)$ and $K_0(z)$ for $D/z_0 = 1600$ obtained by numerical integration are shown in figure 2. As $z \to 0$, $U_0 \sim (u_*/\kappa)\ln[(z+z_0)/z_0]$ and $E_0 \sim u_*^2/\lambda$.

The perturbed velocity components (u, w) and turbulent energy are assumed to have the same period as the bed wave, e.g. $u = u(z)\exp ikx$. Following Benjamin (1959) we shall incorporate part of the effect of the surface undulations into the basic U and W profiles and take

$$U = \overline{U} + u(z^*)\exp ikx^*,$$

$$W = \overline{W} + w(z^*)\exp ikx^*,$$

where $\overline{U} = U_0(z^*)\,\partial z^*/\partial z$, $\overline{W} = -U_0(z^*)\,\partial z^*/\partial x$ and $\overline{U}$ and $\overline{W}$ satisfy the continuity equation (2.8) to first order in $h_0 k$. The turbulent energy is written as

$$E = E_0 + \mathscr{E}(z^*)\exp ikx^*.$$

Then, with the above turbulent closure hypotheses, and linearizing equations (2.6)–(2.9), we have the following, after a certain amount of manipulation. The U momentum equation:

$$-iU_0^2 kh_0 F' + U_0 iku + wU_0' = -ikp_m + \kappa\lambda^{\frac{1}{2}}E_0^{\frac{1}{2}}\left[lu'' + u'\left(l' + \frac{l}{2E_0}\frac{dE_0}{dz^*}\right)\right.$$
$$\left. - k^2 lu + ikw\left(l' + \frac{l}{2E_0}\frac{dE_0}{dz^*}\right) + \frac{1}{2E_0}\left\{\left(U_0'\left(l' - \frac{l}{2E_0}\frac{dE_0}{dz^*}\right) + lU_0''\right)\mathscr{E} + U_0' l\mathscr{E}'\right\}\right]$$
$$+ \kappa\lambda^{\frac{1}{2}}E_0^{\frac{1}{2}}f_1, \quad (2.10)$$

where

$$f_1 = \left[l(ikh_0F' - h_0F''') - (k^2h_0F + h_0F'')\left(l' + \frac{l}{2E_0}\frac{dE_0}{dz^*}\right)\right]U_0$$
$$+ \left[l(k^2h_0F - 3h_0F'') - 3h_0F'\left(l' + \frac{l}{2E_0}\frac{dE_0}{dz^*}\right) + h_0G' + h_0G\frac{1}{2E_0}\frac{dE_0}{dz^*}\right]U_0'$$
$$+ [-3lh_0F' + h_0G]\,U_0''.$$

The W momentum equation:

$$-U_0^2k^2h_0F + ikU_0w = -\frac{dp_m}{dz^*} + \kappa\lambda^{\frac{1}{2}}E_0^{\frac{1}{2}}\left[-k^2lw - ikl u'\right.$$
$$\left. - 2iku\left(l' + \frac{l}{2E_0}\frac{dE_0}{dz^*}\right) + ikl\frac{\lambda^{\frac{1}{2}}}{2E_0}U_0'\mathscr{E}\right] + \kappa\lambda^{\frac{1}{2}}E_0^{\frac{1}{2}}f_2, \quad (2.11)$$

where

$$f_2 = \left[-lk^3h_0F + ilkh_0F'' + 2ikh_0F'\left(l' + \frac{l}{2E_0}\frac{dE_0}{dz^*}\right)\right]U_0$$
$$+ \left[2ikh_0lF' + ikh_0F\left(l' + \frac{l}{2E_0}\frac{dE_0}{dz^*}\right)\right]U_0' + lkh_0FU_0''.$$

The continuity equation

$$iku + \frac{dw}{dz^*} = 0. \tag{2.12}$$

The turbulent energy equation:

$$ikU_0\mathscr{E} + w\frac{dE_0}{dz^*} = \kappa\lambda^{\frac{1}{2}}E_0^{\frac{1}{2}}\left[U_0'^2\left(h_0G + \frac{l}{2E_0}\mathscr{E}\right) + 2l(-h_0U_0'^2F' - U_0U_0'h_0F'' + u'U_0' + U_0'^2h_0F' - U_0U_0'k^2h_0F + ikwU_0')\right] + \frac{\lambda^{\frac{3}{2}}E_0^{\frac{3}{2}}}{\kappa l}\left[\frac{3}{2}\frac{\mathscr{E}}{E_0} - \frac{h_0G}{l}\right] + \kappa\lambda^{\frac{1}{2}}E_0^{\frac{1}{2}}f_3, \tag{2.13}$$

where

$$f_3 = \left[-l\left(k^2 - \frac{1}{2E_0}\frac{d^2E_0}{dz^{*2}} - \left(l' - \frac{l}{2E_0}\frac{dE_0}{dz^*}\right)\frac{1}{2E_0}\frac{dE_0}{dz^*}\right]\mathscr{E} + \left(l' + \frac{l}{E_0}\frac{dE_0}{dz^*}\right)\mathscr{E}' + l\mathscr{E}'' + \frac{d^2E_0}{dz^{*2}}[h_0G - 2h_0F'l] + \frac{dE_0}{dz^*}\left[\frac{h_0G}{2E_0}\frac{dE_0}{dz^*} - 2h_0F'\left(l' + \frac{l}{2E_0}\frac{dE_0}{dz^*}\right) + h_0G' + l(k^2h_0F - h_0F'')\right].$$

Primes denote differentiation which respect to z^*. Length and velocity scales have been non-dimensionalized with D and u_* respectively and $p_m = p + \frac{2}{3}\mathscr{E}_0$. The real and imaginary parts of the linearized perturbed horizontal shear stress are

$$\tau_r = \kappa\lambda^{\frac{1}{2}}E_0^{\frac{1}{2}}\left[l(-2U_0'h_0F' - U_0h_0F'' - U_0k^2h_0F + u_r' - k\omega_i) + \left(h_0G + \frac{l}{2E_0}\mathscr{E}_r\right)U_0'\right]$$

and

$$\tau_i = \kappa\lambda^{\frac{1}{2}}E_0^{\frac{1}{2}}\left[l(u_i' + kw_r) + \frac{l}{2E_0}U_0'\mathscr{E}_i\right].$$

The transformation of the equations to (x^*, z^*) co-ordinates, although considerably complicating the equations, allows a simple specification of the lower boundary conditions. Namely, on $z^* = 0$, the no-slip condition gives

$$u(0) = w(0) = 0 \tag{2.14}$$

and $\partial E/\partial n = 0$, where n is an outward normal to the surface, allowing no diffusion of turbulent energy through the boundary, linearizes to

$$\mathscr{E}'(0) = 0. \tag{2.15}$$

At the upper boundary we will use a Taylor expansion and apply the boundary conditions on the unperturbed free surface. Thus the kinematic condition on

$$\eta = \eta_0 \exp(ikx),$$

the free surface perturbation,

$$U\frac{\partial\eta}{\partial x} = w$$

gives the condition

$$w = ik\frac{U_s}{u_*}\eta_0 \quad \text{on} \quad z^* = D,$$

where U_s is the unperturbed velocity at the surface.

With the hydrostatic approximation this gives

$$w = i\,k\,Fr^2 \frac{u_*}{Us} p_m \tag{2.16}$$

where $Fr^2 = U_s^2/gD$, the Froude number.

The dynamic condition is that the tangential shear stress should vanish. After linearization this gives the condition

$$-\eta_0 l' + \kappa l(u' + ikw) = 0,$$

which gives

$$u' = -ikw + \frac{l'}{\kappa l} Fr^2 \frac{u_*^2}{U_s^2} p_m \quad \text{on} \quad z^* = D. \tag{2.17}$$

We will also take $\partial E/\partial n = 0$ on $z^* = D + \eta$, which linearizes to

$$d\mathscr{E}/dz^* = 0 \quad \text{on} \quad z^* = D. \tag{2.18}$$

With this set of boundary conditions, (2.14)–(2.18), equations (2.10)–(2.13) can be solved numerically using a shooting method (see, for example, Keller 1968). The equations are integrated from one boundary with trial values of the unknown variables at that boundary. A linear combination of solutions to the homogeneous equations is then added to the particular solution of the full equations so that the composite solution satisfies the boundary conditions at the other boundary. This procedure can be applied in either direction. We choose to integrate from the lower to the upper boundary.

For the shorter-length waves considered the depth of flow becomes unimportant. We can therefore consider those waves in a deep turbulent boundary with an undisturbed constant shear stress profile with corresponding logarithmic velocity and linear mixing-length profiles. For a wave with $kD = 4{\cdot}0$ the predictions by the open channel and constant shear stress models for the surface stress, etc. differed by less than 1 %. The results presented for $kD > 4$ in section 4 were obtained with the constant stress model and assuming an infinite depth to the flow.

3. Sediment transport

For low shear rates the dominating mode of transport for sand particles is as bed load and in our study we will neglect any suspended load. Essentially most bed-load formulae can be written in the form

$$q_b = C(\tau_0)^m \tag{3.1}$$

where q_b is the bed-load rate (the mass discharge of sediment) and C a constant dependent on the flow and sediment characteristics. The value of m is taken as $\frac{3}{2}$ in the formulae of Meyer-Peter & Müller (1948) and Bagnold (1956), thus relating the bed-load rate to the fluid power.

Relating the variation with x of q_b to the bed wave height we have the sediment continuity equation, due to Exner (1925),

$$\frac{\partial q_b}{\partial x} = -(1-n)\frac{\partial h}{\partial t}, \tag{3.2}$$

where n is the porosity of the bed. For the wave (2.1) and using equation (3.1) we have, to first order,

$$\sigma = \frac{k^2 C}{1-n} u_*^2 m \frac{\tau^s}{h_0 k}, \tag{3.3}$$

where τ^s is the perturbed tangential bed shear stress (which linearizes to

$$\tau^s = \tau_r(z^* = 0) + i\tau_i(z^* = 0)).$$

The bed is unstable when $\sigma_i > 0$. This requires $\tau_i^s > 0$, i.e. the maximum in the shear stress and thus sediment transport rate to be upstream of the crest. In physical terms, if the sediment transport rate is decreasing over the crest then deposition will take place, while erosion will occur if it is increasing.

We shall see later that in order to obtain a maximum in the growth rate of bed waves we need to restrict the growth of waves to a finite wavenumber. As shown experimentally by Lysne (1969) gravity has a significant contribution to the force on the sediment when the bed is sloping. This will have a stabilizing effect on the bed wave because the effects of gravity will reduce the transport rate of sediment towards the crest from upstream and increases it away from the crest, downstream. Fredsøe (1974) introduces this effect by relating the additional force due to gravity to the bed slope. We shall follow Fredsøe and take the perturbed bed load to be proportional to $u_*^2(\tau^s - \beta \partial h/\partial x)$, where β is taken to be constant. Then equation (3.3) becomes

$$\sigma = Ak^2\left(\frac{\tau^s}{h_0 k} - i\beta\right), \tag{3.4}$$

where A is a constant dependent on the unperturbed shear stress and the nature of the sediment.

We can provide estimates for A and β by applying a specific transport formula. Bagnold (1956) relates the rate of work done in pushing the bed load along the bed against frictional resistance to the power in the flow available to move the sediment. For a bed of inclination α to the horizontal this gives

$$q_b = \frac{8{\cdot}5}{\gamma g} e_b \frac{\tau_0^{\frac{1}{2}}(\tau_0 - \tau_{cr})}{(\tan\phi + \tan\alpha)\cos\alpha}, \tag{3.5}$$

where e_b is an efficiency factor of order 0·1, ϕ the angle of frictional resistance, τ_{cr} the critical shear stress for sediment movement and $\gamma = (\rho_s - \rho)/\rho$ with ρ_s and ρ the density of the sediment and fluid respectively.

Linearizing equation (3.5) with respect to wave slope gives equation (3.4) with

$$\left.\begin{aligned} A &= \frac{8{\cdot}5 e_b}{\gamma g \tan\phi}\left(\frac{3\tau_0 - \tau_{cr}}{2\tau_0^{\frac{1}{2}}}\right)\cdot\frac{1}{1-n} \\ \text{and} \quad \beta &= 1/\tan\phi. \end{aligned}\right\} \tag{3.6}$$

In an earlier paper Bagnold (1954) describes experiments on the shearing of sand grains. He distinguishes two limiting cases, where the stresses between grains are transmitted by the fluid viscosity and where this is done wholly by particle–particle

interactions. From his experimental results he obtains the following limits for the angle of frictional resistance, ϕ,

$$0{\cdot}75 > \tan\phi > 0{\cdot}32, \tag{3.7}$$

with $\tan\phi$ decreasing for increasing shear stress and grain size.

This gives values of β between

$$1{\cdot}3 < \beta < 3.1. \tag{3.8}$$

4. Results

We shall consider the limiting case of zero Froude number, i.e. assume the free surface to be plane. The results for non-zero Froude number, discussed later in this section, show that the results of the analysis are approximately unchanged for $Fr < 0{\cdot}25$ (figure 10), a condition which is adequately satisfied by most large rivers and the sea.

The flow over the bed wave, in terms of the wave slope $h_0 k$, is dependent on the two non-dimensional parameters kD and D/z_0. Profiles of the real and imaginary parts of the perturbed shear stress, turbulent energy and pressure plotted against

$$\zeta = \ln[(z+z_0)/z_0]$$

are shown in figures 3 and 4 for a typical case with $kD = 1$ and $D/z_0 = 1600$. Taking, say, $z_0 = 0{\cdot}5$ cm, this corresponds to a wave of wavelength 50 m and a flow depth of 8 m. At the bed the stress maximum is upstream of the crest, with a phase lag of $\theta_\tau = 30{\cdot}2°$. There is also an additional elevated extremum approximately 180° out of phase with the bed and height $0{\cdot}25D$ above the bed. The pressure remains approximately constant with depth and 175° out of phase with the bed.

The results of the present model can be compared with those of Townsend (1972) for flow over water waves by taking a constant unperturbed stress profile and letting the depth of flow tend to infinity. The only results he presents for a fixed wave are with $R = -\ln(kz_0) = 8$. He obtains bed stress values of $\tau_r^s/h_0 k = 4{\cdot}28$, $\tau_i^s/h_0 k = 1{\cdot}69$, which gives a phase lag of $\theta_\tau = 21{\cdot}5°$. This compares with $\tau_r^s/h_0 k = 4{\cdot}21$, $\tau_i^s/h_0 k = 2{\cdot}34$ and $\theta_\tau = 29{\cdot}1°$ for our model. This discrepancy may be due to Townsend's treatment of the lower boundary but is also due to the different turbulence closures of the two models.

We are interested in the stability of the bed and thus in the value of the imaginary part of the bed shear stress (equation (3.4)). In figure 5, $\tau_i/h_0 k\rho u_*^2$ is plotted against kz_0, for $D/z_0 = 10^4$ and 10^5. We note that there are two maxima in each curve, at $kz_0 = 5{\cdot}8 \times 10^{-6}$ ($kD = 0{\cdot}058$) and $kz_0 = 7{\cdot}0 \times 10^{-3}$ for $D/z_0 = 10^4$ and at $kz_0 = 4.4 \times 10^{-7}$ ($kD = 0{\cdot}044$) and $kz_0 = 7{\cdot}0 \times 10^{-3}$ for $D/z_0 = 10^5$. We shall treat the two maxima separately.

(*a*) *Ripple mode*

The second of the two maxima in $\tau_i^s/\rho h_0 k u_*^2$ is independent of the flow depth and we shall use the results of the model with an unperturbed constant stress layer and infinite depth. The flow is then only dependent on kz_0. From equation (3.4) the growth rate of the bed wave is proportional to $\omega_r = [(kz_0)^2/u_*^2]\,(\tau_i/h_0 k - \beta)$. The results for

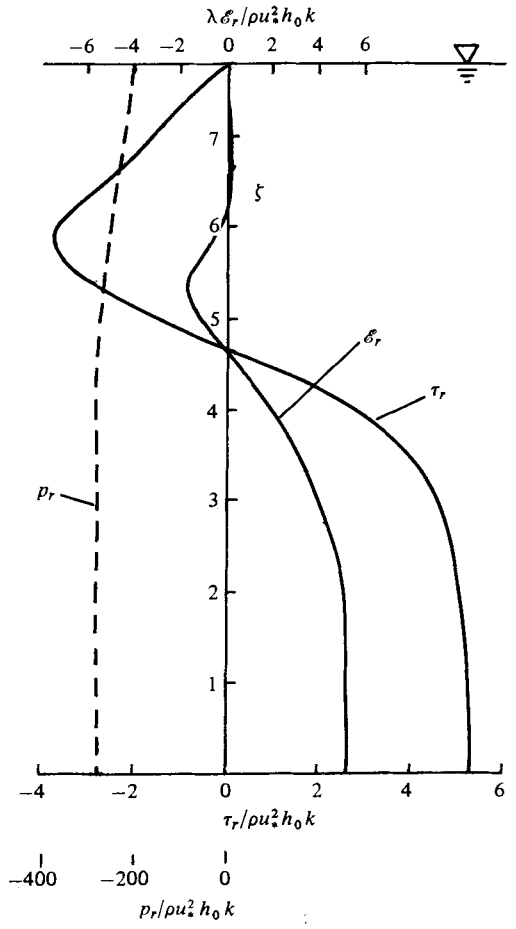

FIGURE 3

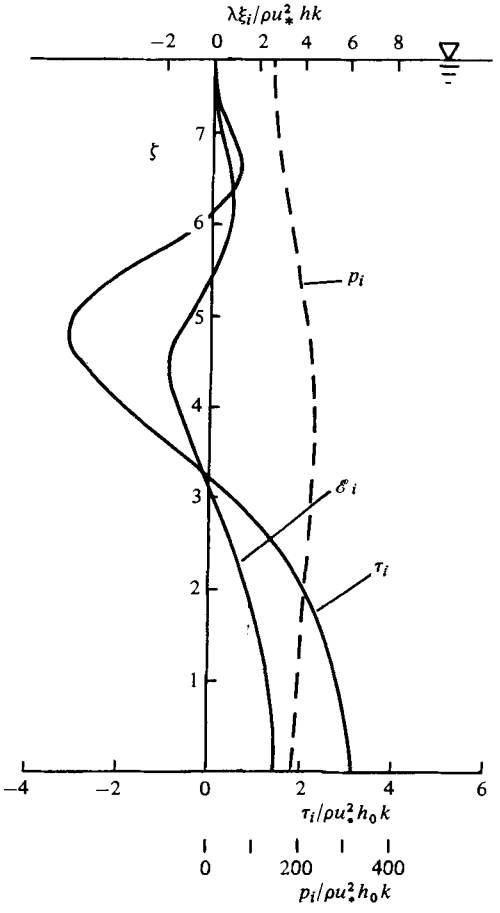

FIGURE 4

FIGURE 3. Vertical profiles of the real parts of the perturbed stress, τ_r, turbulent energy, $\mathscr{E}_r$, and pressure, p_r; $kD = 1{\cdot}0$, $D/z_0 = 1600$.

FIGURE 4. Vertical profiles of the imaginary parts of the perturbed stress, τ_i, turbulent energy, $\mathscr{E}_i$, and pressure, p_i; $kD = 1{\cdot}0$, $D/z_0 = 1600$.

varying β are shown in figure 6. For $\beta > 2{\cdot}9$ the bed is always stable as $\tau_i/h_0 k - \beta$ is negative. We note that for $\beta = 0$ the growth rate increases monotonically with kz_0. However, for a non-zero value of $\beta < 2{\cdot}9$ the growth rate attains a maximum positive value for a finite value of kz_0, giving a preferred wavelength at which we would expect a disturbance to grow. Table 1 gives the wavenumber for which the growth rate is a maximum together with the maximum growth rate for β varying between 1·4 and 2·9. This gives the range

$$0{\cdot}007 < kz_0 < 0{\cdot}16 \tag{4.1}$$

with kz_0 increasing for decreasing β.

There is therefore an unstable bed wave mode independent of the depth of flow, which we will classify as a 'ripple' mode dependent on the roughness length z_0 and the value of β.

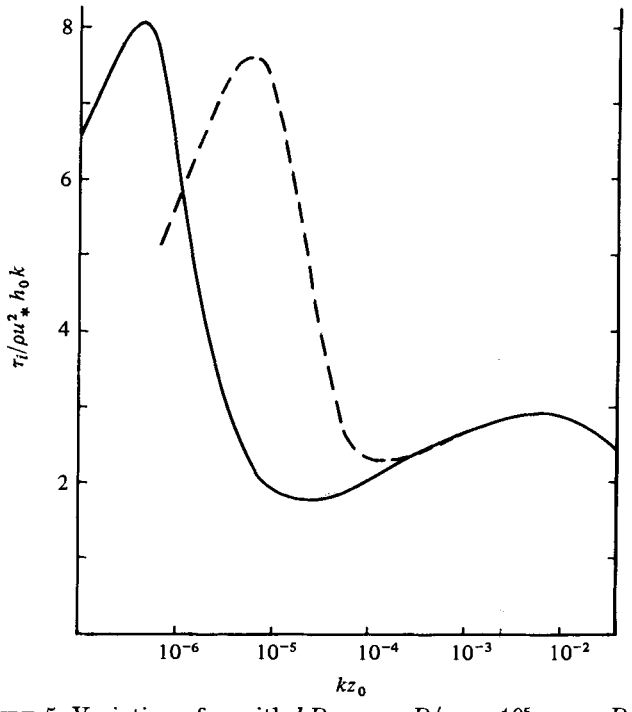

FIGURE 5. Variation of τ_i with kD; ——, $D/z_0 = 10^5$; – – –, $D/z_0 = 10^4$.

(*b*) *Dune mode*

For small values of kD the depth of the flow becomes important and the first maximum in $\tau_i^s/h_0 k\rho u_*^2$ (figure 5) is dependent on kD. The growth rate $\omega_d = [(kD)^2/u_*^2](\tau_i/h_0 k - \beta)$, now non-dimensionalized with respect to depth, plotted against kD is shown in figure 7 for various values of D/z_0 with $\beta = 2{\cdot}8$. For the curves plotted, with $D/z_0 > 10^3$ a maximum occurs at a value of kD which varies with D/z_0. This we will classify as the dune mode of growth. The curves will rise again, not plotted, to a second maximum at $kz_0 = 0{\cdot}07$ corresponding to the ripple mode. For $D/z_0 = 10^2$ the dune and ripple modes have coalesced, giving only a single maximum in the growth rate curve. As β decreases, for a fixed value of D/z_0, the dune mode disappears leaving only the ripple mode. Figure 8 shows the results with $\beta = 2{\cdot}4$. The wavenumber at which the dune maximum occurs, together with the growth rate, is given in table 2, for a number of values of β and D/z_0. The value of kD is found to decrease with an increase in D/z_0, i.e. for a fixed value of z_0 the wavelength increases with increasing depth.

We therefore find two modes of instability of a plane erodible bed, one whose wavelength is dependent on the surface roughness of the bed, corresponding to the formation of ripples, the other dependent primarily on the depth of flow, corresponding to the formation of dunes. Both instabilities can occur singly or together depending on the values of β and D/z_0. A comparison of the results of the theory with observation is carried out in the next section.

Engelund & Fredsøe's (1974) results, using a constant eddy viscosity, do not show a second unstable region corresponding to ripples. Smith (1970) obtains asymptotic solutions for the growth rate with a constant eddy-viscosity model for large and small

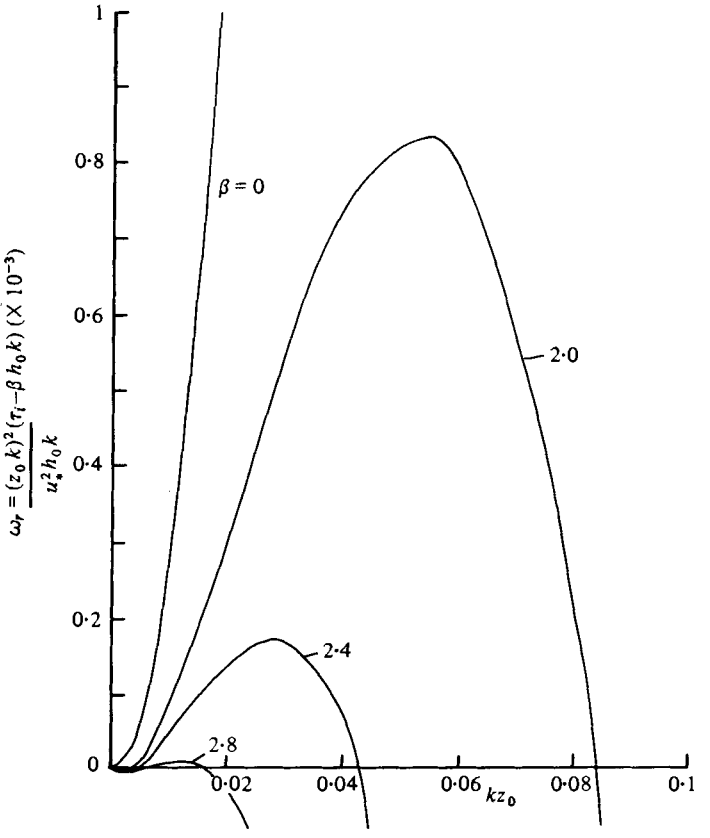

FIGURE 6. Growth rate of ripple mode, ω_r, for various values of β.

	β				
	0	1·4	2·0	2·4	2·8
Growth rate × 10^{-3}	—	5·35	0·83	0·17	0·01
kz_0	—	0·155	0·054	0·029	0·011

TABLE 1. Growth rate, $\omega_r = [(z_0k)^2/h_0ku_*^2]\,(\tau_i - \beta h_0 k)$, and wavenumber of fastest-growing ripple mode.

waves. In terms of the bed shear stress he finds that $\tau_i^s \sim \frac{4}{35}Re$ for $kD \ll 1$ and $\tau_i^s \sim \frac{3}{2}Re/kD$ for $kD \gg 1$, where $Re = U_0D/K$. For intermediate values of kD Smith presents computed results with $Re = 500$ which show $\partial\tau_i^s/\partial k < 0$ for all $kD > 0$. Thus the τ_i, kD curve has only one maximum, at $kD = 0$, and for a given value of β the constant eddy-viscosity model will predict only one mode of instability.

The effect of varying the Froude number, Fr, on the results for $\tau_i^s/h_0k\rho u_*^2$ plotted against kD are shown in figure 9 with $D/z_0 = 3 \times 10^3$ and $\beta = 2{\cdot}8$. For $kD > 3{\cdot}5$ the stress is unaffected by variation in Fr. Below this value of kD the effect of increasing Fr is very marked. A sharp dip in the curve appears for increasing Fr with an increase

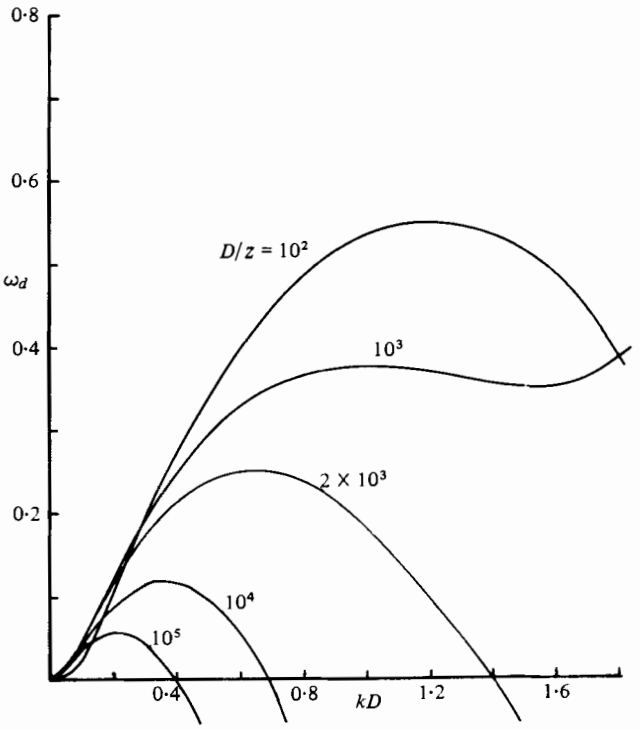

FIGURE 7. Growth rate of dune mode, ω_d, for various values of D/z_0; $\beta = 2{\cdot}8$.

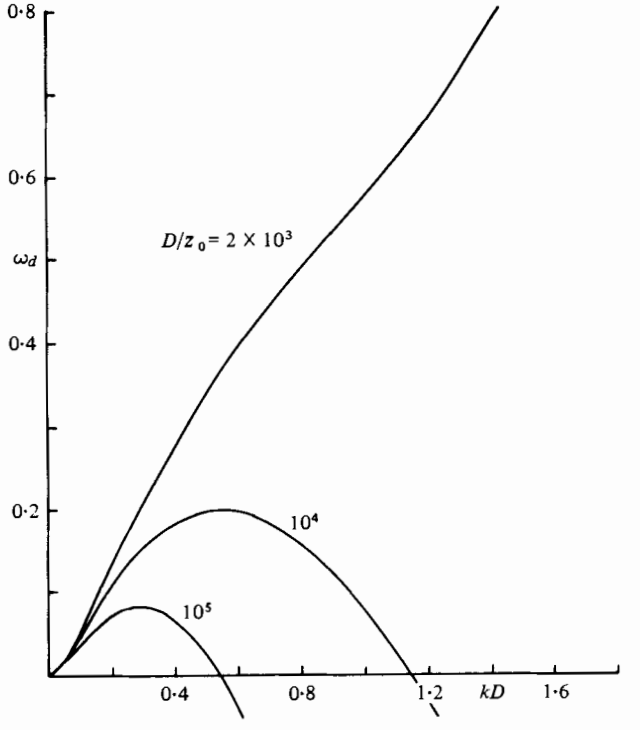

FIGURE 8. Growth rate of dune mode, ω_d; $\beta = 2{\cdot}4$.

	z_0/D	β 2·0	2·4	2·6	2·8
Growth rate	10^{-5}	0·13	0·08	0·07	0·06
kD		0·41	0·29	0·26	0·23
Growth rate	10^{-4}	–	0·20	0·15	0·12
kD		–	0·59	0·44	0·36
Growth rate	5×10^{-4}	–	–	0·39	0·25
kD		–	–	1·54	0·63
Growth rate	10^{-3}	–	–	–	0·38
kD		–	–	–	1·00

– No dune mode.

TABLE 2. Growth rate, $\omega_d = [(kD)^2/h_0 k u_*^2]\,(\tau_i - \beta h_0 k)$, and wavenumber of fastest-growing dune mode.

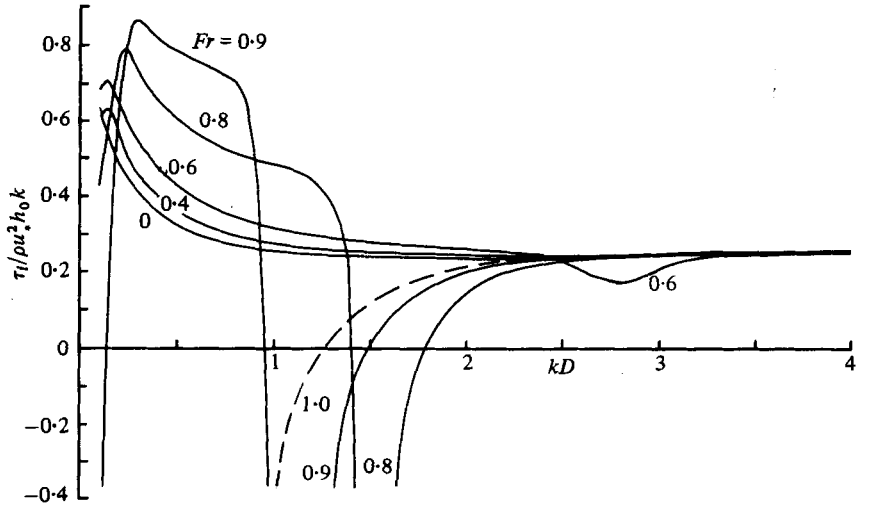

FIGURE 9. Imaginary part of perturbed surface stress, τ_i, for various values of the Froude number, Fr; $D/z_0 = 3 \times 10^8$, $\beta = 2{\cdot}8$.

in the maximum at low wavenumbers. At $Fr = 1$ a transition occurs when the maximum in τ_i^s disappears with $\tau_i^s < 0$ for $kD < 1{\cdot}2$.

Figure 10 is a stability diagram from the results showing the regions of stable and unstable bed-waves. For $Fr < 0{\cdot}25$ the stability criterion is almost constant. Above $Fr \simeq 1{\cdot}0$ no dunes will exist marking the transition of the bed from a dune to a flat bed regime. The ripple region of unstable waves, which for $\beta = 2{\cdot}8$ is $0{\cdot}006 < kz_0 < 0{\cdot}016$ ($18 < kD < 48$) with a maximum growth rate at $kz_0 = 0{\cdot}011$, is unaffected by variations in Fr.

The dune region is similar in shape to those produced by Engelund & Fredsøe (1974), with the present results being extended to low Froude numbers.

As we should expect the present model does not predict the existence of antidunes. The work of Engelund & Fredsøe suggests that suspended sediment is required in the

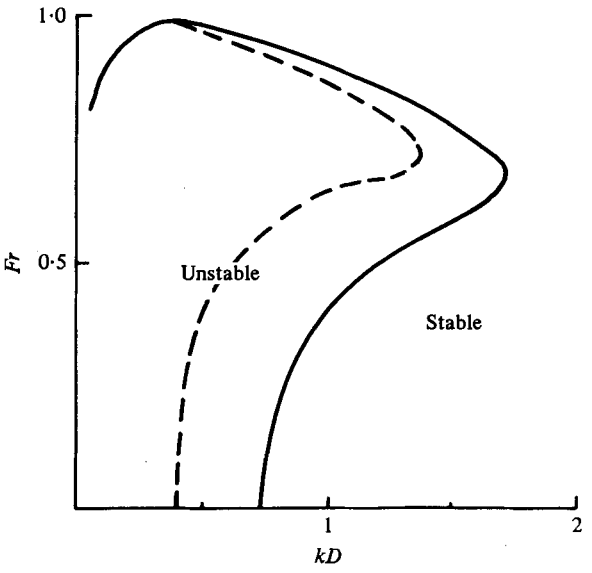

FIGURE 10. Stability limits to the formation of dunes; $D/z_0 = 3 \times 10^3$, $\beta = 2{\cdot}8$. The dashed curve corresponds to the fastest-growing wavenumber.

model to account for the formation of antidunes. They also argue that the transition region from dune to flat bed regimes is strongly affected by the balance between bed load and suspended load, thus requiring accurate predictions of both forms of transport. The stability boundaries would therefore be affected by the inclusion of suspended sediment for the higher-Froude-number flows.

5. Comparison with observation

We shall be comparing the results of the linear analysis giving the initial growth of the bed wave, with observations of fully developed waves. For low-Froude-number flows Fredsøe & Engelund (1975) find that the wavelength of dunes is nearly constant during their growth, although there is a significant increase in the wavelength at higher Froude numbers. However, as observed by many authors, ripples lengthen during their development, their final wavelength being controlled by the separated flow over the developed wave. Again we shall consider the two modes of growth separately.

(*a*) *Ripples*

Yalin (1964), using experimental results from flume studies made by a number of authors, estimates that the wavelength of ripples, λ_r, is given approximately by

$$\lambda_r = 1000d, \tag{5.1}$$

where d is the grain diameter of the sediment particles. Allen (1970) obtains the same result. However, the scatter in the data is large. Ratios of λ_r/d as low as 400 and as high as 3000 appear even over the narrow range of grain sizes investigated (0·19–0·54 mm).

The range of wavenumber for the ripple mode given by equation (4.1) cover over one order of magnitude for a factor-two variation in the value of β. In terms of the wavelength this is

$$50z_0 < \lambda_r < 1000z_0. \tag{5.2}$$

For a hydraulically rough flow Nikuradse (1933) found the roughness length to be given approximately by

$$z_0 = d/30.$$

In a similar series of experiments of water flow over fixed sand grains the value was later modified by Kamphuis (1974) to

$$z_0 = d/15. \tag{5.3}$$

Using this value for the roughness length, expression (5.2) gives

$$3d < \lambda_r < 60d, \tag{5.4}$$

which is clearly an order of magnitude or so too small for observed ripples (but see the discussion in § 6).

The experiments of Nikuradse and Kamphuis were carried out with an artificially smoothed fixed bed of a single grain size. For flows above a mobile bed with the shear stress above the critical stress for particle movement the moving sediment will effect the value of z_0. Extending the work of Owen (1964) for air flow over sand to water flow, Smith & McLean (1977) relate the roughness length to the height of the bed-load layer. They obtain

$$z_0 = \alpha_0(\tau_0 - \tau_{cr})/(\rho_s - \rho)g + z_n \quad \text{for} \quad \tau_0 > \tau_{cr},$$

where z_n is the roughness length given by Nikuradse's work. Using data from the Columbia River with a medium grain size of 0·33 mm, a value of $\alpha_0 = 26{\cdot}3$ gives a good agreement with their observations. With values of u_* varying between 1·7 and 4·6 cm s^{-1} this gives values of z_0 between 0·01 and 0·32 cm, an order of magnitude higher than the Nikuradse roughness length.

Taking a mean value of $z_0 = 4{\cdot}5d$, expression (5.2) becomes

$$203d < \lambda_r < 4050d. \tag{5.5}$$

With this order-of-magnitude increase in z_0 due to moving sediment the theory therefore predicts a wavelength comparable to that of observed ripples.

(*b*) *Dunes*

Results from flume experiments suggest that the wavelength of dunes is given approximately by

$$\lambda_d = 2\pi D \tag{5.6}$$

(see, for example, Allen 1970). However, the range of depths covered is small ($D \lesssim 0{\cdot}5$ m). From field observations Allen (1970) suggests that a better fit of the data for deeper flows is given by

$$\lambda_d = 1{\cdot}16D^{1{\cdot}55}, \tag{5.7}$$

where λ_d and D are given in metres.

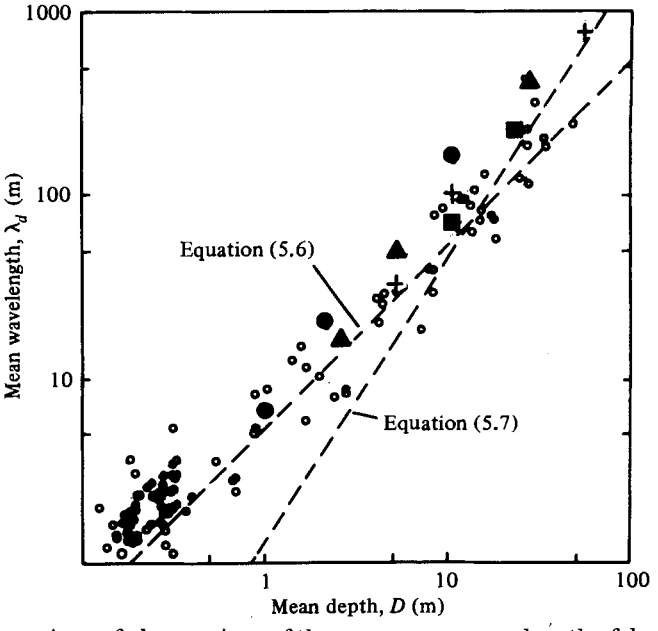

FIGURE 11. Comparison of observations of the group mean wavelength of dunes from flume, river and marine environments (taken from Jackson 1976) with the model's results: ○, observations; ●, $z_0 = 0{\cdot}1$ cm; ▲, $z_0 = 0{\cdot}25$ cm; +, $z_0 = 0{\cdot}5$ cm; ■, $z_0 = 1{\cdot}0$ cm.

Figure 11 (taken from Jackson (1976)) shows observational results of the group mean wavelength of dunes plotted against the mean depth of flow for flume, river and marine environments (see Jackson's table 3 for the sources of data) together with equations (5.6) and (5.7). For the larger flow depths the data show an increase in the ratio λ_d/D for increasing D.

Also plotted in figure 11 are the results of the present model with $\beta = 2{\cdot}8$ for values of z_0 from 0·25 cm to 1·0 cm. The value of z_0 is now governed by the effective roughness of a rippled bed. For a given D/z_0 these lie on a straight line parallel to $\lambda_d = 2\pi D$, with the ratio λ_d/D increasing for increasing D/z_0 as exhibited by the data. It should be noted that the results are sensitive to the value of β (table 2) and that the scatter of the data presented in figure 11 can be more than covered by varying β.

6. Discussion

The development time of the bed wave, T_b, is $1/\sigma_i$, where σ_i is given by equation (3.4). Considering the ripple case, taking $u_* = 5$ cm s^{-1}, $z_0 = 0{\cdot}02$ cm and a ripple of wavelength $L = 12$ cm, then $\sigma_i \sim 1{\cdot}5 \times 10^{-3}$ s^{-1} and $T_b \sim 600$ s. Assuming the development time of the flow to be given by $T_f \sim UL/\tau$ (where the depth of the flow affected by the bed wave is assumed to be $O(L)$) gives $T_f \sim 10$ s. For the dune case again taking $u_* = 5$ cm s^{-1} with a flow depth $D = 10$ m, then $T_b \sim 10$ days. The flow development time in a unidirectional flow is given by $T_f \sim UD/\tau$, i.e. $T_f \sim 30$ min. In a tidal flow $T_f \sim 12$ h. In both the dune and the ripple cases $T_f \ll T_b$. Thus our assumption of neglecting the movement of the bed in calculating the flow is valid.

Williams & Kemp (1971) observed the growth of ripples from an initially flat bed

comprised of sand 0·14 mm and 0·50 mm in diameter. Using a knife-edge lighting arrangement they were able to detect small variations in the bed elevation. The time scale of development from a flat bed to ripples a few grain diameters in height was approximately 100 s, comparing well with our result of 600 s.

We can also calculate the forward translational velocity of the bed wave, given by σ_r/k. For the parameters given above this gives for the ripple a value of $\sim 3 \times 10^{-3}$ cm s^{-1} and for the dune $\sim$ 1 m/day in a unidirectional flow.

The scour and deposition process for ripple formation proposed by Williams & Kemp (1971) assumes the bed to be initially disturbed by a 'burst' of high shear stress. However, 'bursts' are three-dimensional and, in the sea, have dimensions much greater than the wavelength of the ripples. The mechanism of Williams & Kemp does not account therefore for the two-dimensionality, at least initially, of ripple fields. In the author's view it seems unlikely that such a mechanism can have such a drastic effect on the flow and bed unless there is some basic instability of the bed giving a definite wavelength for ripple growth. From the results of the analysis it is postulated therefore that, although the bursting phenomenon may be a possible triggering mechanism, ripples are formed by an unstable mode of the bed responding to some disturbance of the bed, rather than propagating downstream by a scour and deposition process.

Once the ripple has attained some finite size the effective roughness of the bed will be increased, being dependent on the dimensions of the developed ripple. Observed values of z_0 over rippled beds are typically an order of magnitude higher than those observed for plane beds. We can expect the results of the model to still hold and, using equation (4.1), the model can be extended to predict the formation of a second ripple dependent on the 'roughness' of the first. In this way a hierarchy of ripples can be built up, each increasing in wavelength until some limiting factor such as the depth of flow becomes important.

It is now possible to argue that we can use the value of the surface roughness due to Nikuradse to predict the growth of ripples of an observed wavelength, since using equation (5.3) for z_0 predicts the growth of 'micro-ripples' which, by increasing z_0, trigger the growth of larger ripples. This is similar in concept to the 'primary ripples' of Bagnold (1956), although the mechanism of the instability is different. However, whether this is the case or that the moving sediment itself increases z_0 would need some very carefully controlled experiments to clarify.

Using the above extension to the model we can also account for the existence of larger-wavelength mega-ripples observed in deeper flows. Taking a value of $z_0 = 0{\cdot}5$ cm for a rippled bed of wavelength 20 cm, then the mid-range of equation (5.2) predicts a mega-ripple of wavelength 3 m comparable to observed waves (see, for example, Langhorne 1973). It should be noted that the mechanism of Williams & Kemp (1971) would not predict the formation of larger ripples nor the 'spectral gap' between the two distinct wavelengths.

The results of the analysis are strongly dependent on the value of β. In particular the model predicts that ripples will not form for $\beta > 2{\cdot}9$. Using the theory of Bagnold (1956) for the sediment transport we find that β increases for increasing shear stress and grain size (equations (3.6) and (3.7)). An interesting feature of ripples is that their existence appears to be restricted to sediment finer than a definite mean size, in qualitative accordance with the theory. From flume experiments Moss (1972) gives

a value for the grain size limit of 0·92 mm. Bagnold (1956) presents experimentally determined values of $\tan\phi$ for a number of different grain sizes with low shear rates. Assuming that $\beta = 1/\tan\phi$ [equation (3.6)] and using table 2 from Bagnold (1956) for $\tan\phi$, this value of grain-size limit would give a critical value of $\beta \simeq 2{\cdot}0$ for ripple formation, although there is a great deal of uncertainty in this value.

For an increasing flow, ripples are observed to be 'washed out' above some critical shear stress, again in qualitative agreement with the theory, although no direct quantitative comparison can be made at present. It should however be noted that for increasing shear stresses the suspended load will become more important. Engelund & Fredsøe (1974) show that the suspended load has a stabilizing effect on the bed wave and therefore the stability of the bed will also be dependent on the balance between the bed and suspended load.

7. Conclusions

The results of the linear stability analysis with particular regard given to the turbulent flow close to the surface show an erodible bed to be unstable at two modes dependent on the roughness of the bed and the depth of the flow respectively. The results depend on the two parameters z_0, the roughness length of the bed, and β, the effect of the local bed slope on the bed-load transport. With a careful choice of z_0 and β the comparison of the results of the analysis with observation is good for both ripples and dunes, and strongly suggests that ripples are formed by an instability mechanism. Clearly, however, before any firm conclusions can be drawn from the analysis, a better understanding is needed of the parameterization of the roughness of the bed when the sediment is moving and the effects of the local bed slope on the bed load.

This work forms part of the author's Ph.D. thesis submitted to the University of Southampton. The author would like to express his thanks to his research supervisor Dr P. A. Taylor for much encouragement and advice and the Natural Environment Research Council for financial support.

REFERENCES

ALLEN, J. R. L. 1970 *Physical Processes of Sedimentation*. Elsevier.

BAGNOLD, R. A. 1954 *Proc. Roy. Soc.* A **225**, 49.

BAGNOLD, R. A. 1956 *Phil. Trans. Roy. Soc.* A **249**, 235.

BENJAMIN, T. B. 1959 *J. Fluid Mech.* **6**, 161.

BRADSHAW, P., FERRIS, P. H. & ATWELL, N. P. 1967 *J. Fluid Mech.* **28**, 593.

ENGELUND, F. 1970 *J. Fluid Mech.* **42**, 225.

ENGELUND, F. & FREDSØE, J. 1974 *Tech. Univ. Denmark, Inst. Hydrodyn. and Hydraulic Engng, Series Paper* 4.

EXNER, F. M. 1925 *Sitzber. Akad. Wiss. (Wien)* **3–4**, 165.

FREDSØE, J. 1974 *J. Fluid Mech.* **64**, 1.

FREDSØE, J. & ENGELUND, F. 1975 *Tech. Univ. Denmark, Inst. Hydrodyn. and Hydraulic Engng, Series Paper* 8.

JACKSON, R. G. 1976 *J. Fluid Mech.* **77**, 531.

KAMPHUIS, J. W. 1974 *J. Hydraulic Res.* **12**, 193.

KELLER, H. B. 1968 *Numerical Methods for Two-point Boundary Values Problems*. Waltham, Mass.: Blaisdell.

KENNEDY, J. F. 1963 *J. Fluid Mech.* **16**, 521.
LANGHORNE, D. N. 1973 *Marine Geol.* **14**, 129.
LIU, H. K. 1957 *Proc. A.S.C.E.* **83** (HY2), 1197.
LYSNE, D. K. 1969 *Proc. A.S.C.E.* **95** (HY6), 1835.
MEYER-PETER & MÜLLER, R. 1948 *Inter. Ass. Hydr. Res., 2nd Meeting, Stockholm.*
MILES, J. W. 1957 *J. Fluid Mech.* **3**, 185.
MOSS, A. J. 1972 *Sedimentology* **18**, 159.
NIKURADSE, J. 1933 *V.D.I. – Forschungsheft* no. 361.
OWEN, P. R. 1964 *J. Fluid Mech.* **20**, 225.
RAUDKIVI, A. J. 1966 *J. Fluid Mech.* **26**, 507.
REYNOLDS, A. J. 1976 *Nordic Hydrology* **7**, 161.
RICHARDS, K. J. 1978 Ph.D. thesis, University of Southampton.
RODI, W. 1978 *Univ. Karlsruhe Rep.* SFB 80/T/127.
SMITH, J. D. 1970 *J. Geophys. Res.* **75**, 5928.
SMITH, J. D. & MCLEAN, S. R. 1977 *J. Geophys. Res.* **82**, 1735.
TAYLOR, P. A. 1977 *Boundary-Layer Met.* **11**, 439.
TAYLOR, P. A., RICHARDS, K. J. & NUNES, R. A. 1978 In *Turbulent Fluxes Through the Sea Surface, Wave Dynamics, and Prediction* (ed. A. Favre & K. Hasselman). Plenum.
TOWNSEND, A. A. 1972 *J. Fluid Mech.* **55**, 719.
WILLIAMS, P. B. & KEMP, P. H. 1971 *Proc. A.S.C.E.* **97** (HY4), 505.
YALIN, M. S. 1964 *Proc. A.S.C.E.* **90** (HY5), 105.